Large scale numerical investigation of excited states in poly(phenylene)

Robert J. Bursill[1*] and William Barford[2**]
[1] *School of Physics, The University of New South Wales, Sydney, NSW 2052, Australia.*
[2] *Department of Physics and Astronomy, The University of Sheffield, Sheffield, S3 7RH, United Kingdom.*

A density matrix renormalisation group scheme is developed, allowing for the first time essentially exact numerical solutions for the important excited states of a realistic semi-empirical model for oligo-phenylenes. By monitoring the evolution of the energies with chain length and comparing them to the experimental absorption peaks of oligomers and thin films, we assign the four characteristic absorption peaks of phenyl-based polymers. We also determine the position and nature of the nonlinear optical states in this model.

The phenyl-based conjugated polymers have attracted immense interest from physicists and chemists as a result of the discovery of electroluminescence in poly(phenylenevinylene) (PPV) [1]. In particular, a great deal of theoretical and experimental effort has been devoted to understanding the important neutral excitations driving nonlinear optical processes, the positions of triplet states and the nature of exciton binding and decay [2–6]. Correlation between π-electrons has proved to be important in obtaining an accurate description of excited states in conjugated systems. It is thus desirable to have accurate numerical solutions of correlated electron models for these systems (without recourse to uncontrolled approximation schemes such as configuration interaction approximation schemes, or perturbative schemes starting from a noninteracting molecular orbital or k-space band description). In this paper we provide, for the first time, accurate results for a realistic semi-empirical model for poly(phenylene) and its oligomers, a model system for phenyl-based conjugated polymers.

As our starting point for describing poly(phenylene), we adopt the Pariser-Parr-Pople (P-P-P) model [7],

$$\begin{aligned}\mathcal{H} = &- \sum_{<ij>\sigma} t_{ij} \left[c^\dagger_{i\sigma} c_{j\sigma} + \text{h.c.} \right] \\ &+ U \sum_i \left(n_{i\downarrow} - 1/2 \right) \left(n_{i\downarrow} - 1/2 \right) \\ &+ \frac{1}{2} \sum_{i \neq j} V_{ij} (n_i - 1)(n_j - 1), \end{aligned} \tag{1}$$

where $<>$ represents nearest neighbors, $c_{i\sigma}$ destroys a π-electron on conjugated carbon atom i, $n_{i\sigma} = c^\dagger_{i\sigma} c_{i\sigma}$ and $n_i = n_{i\uparrow} + n_{i\downarrow}$. We use the Ohno parameterisation for the Coulomb interaction, $V_{ij} = U/\sqrt{1 + (U r_{ij}/14.397)^2}$, where r_{ij} is the inter-atomic distance in Å and $U = 10.06$ eV [8]. The transfer integrals (t_{ij}) and bond lengths are 2.539 eV and 1.4 Å respectively for phenyl bonds, and 2.22 eV and 1.51 Å respectively for single bonds [8]. In the following we consider oligophenyls of N repeat units (phenyl rings), as depicted in Fig. 3.

When solved accurately, the P-P-P theory has proved remarkably accurate in describing many of the low-lying excitations in a wide range of conjugated molecules [8,9]. Given such debates as to the nature of exciton binding in PPV and the related issues of interpreting various spectral features [2–6], it is intriguing as to what the P-P-P theory predicts for large phenyl systems. Exact diagonalisation is currently restricted to systems with two phenyl rings. The advent of the density matrix renormalisation group (DMRG) method [10] has been fortuitous in that it has the potential to provide effectively exact numerical solutions of the P-P-P theory for systems with hundreds of conjugated carbon atoms. The DMRG has obstensively been restricted to systems with acetylene-like (simple, linear chain) geometry [11,12] to date. This is because it has not been possible to keep a complete basis for the phenyl repeat unit (4096 basis states) as well as sufficient system and environment block states. In this work we develop an accurate method for treating the phenyl block based on local Hilbert space optimisation [12,13].

Our approach starts with the assumption that an optimised local Hilbert space prepared in a small system should also be suitable for a large system. We employ the following procedure:

1. The P-P-P model is solved exactly for the 12-site ($N = 2$) biphenyl molecule. The right-hand ring acts as the environment for the left-hand ring. A reduced density matrix for the left-hand ring is constructed by performing a partial trace of the target state(s) projection operator over the states of the right-hand ring. The m_A optimal states for the left-hand ring (i.e. the optimised local Hilbert space) are those density matrix eigenstates with the highest eigenvalues. These are the natural many body states of the phenyl ring at the end of an oligophenylene molecule, in analogy to the natural one-electron orbitals of quantum chemistry.

2. For phenyl rings added to the middle of the lattice during the DMRG iterations (i.e. rings with

neighbours to the left and right), we apply periodic boundary conditions to the biphenyl molecule to again construct an optimal basis, of which the m_B most important states are retained. We note that this method of determining a suitable repeat unit Hilbert space from a small, exactly diagonalisable system is employed at the first stage of the "four-block" DMRG method [14].

3. Once the local Hilbert space has been optimised the usual inifinite lattice DMRG approach is used to build up oligophenyls. We use a three-block infinite lattice method, the environment block being the reflected system block. This enables us to apply the full symmetries of the Hamiltonian, which are the two planes of reflection, and particle-hole and spin-flip symmetries. We use the symbols A_g and B_{1u} to denote states that are symmetric under long-axis reflection, the A_g states being symmetric under short axis reflection, the B_{1u} states being antisymmetric under short axis reflection (polarised along the molecular axis). We use the symbol B_{2u} to denote states that are polarised perpendicular to the molecular axis, i.e., states which are symmetric under long axis reflection and antisymmetric under short axis reflection. The spin-flip symmetry is used to distinguish singlet and triplet states, i.e., singlet states in the A_g sector are denoted ${}^1A_g$ whilst triplet states are denoted ${}^3A_g$. Finally, the particle-hole symmetry of states is denoted by a "+" or "−" superscript. For example, the second lowest state in the A_g singlet sector with positive particle-hole symmetry is denoted $2{}^1A_g^+$.

4. Oligophenyls with an even number of phenyl rings are constructed by performing DMRG iterations with no repeat unit (i.e., just with a system and environment block).

We embellish the basic approach described above with some further optimisations that serve to accelerate the convergence of energies with m_A and m_B. Fig. 1 shows the construction of the initial phenyl bases: the end phenyl unit basis (for the first system block) is derived from the exact diagonalisation of biphenyl with open boundary conditions; the initial middle phenyl unit basis is derived from exactly diagonalising biphenyl with periodic boundary conditions. However, before using the middle block basis in DMRG iterations it pays to perform an improvement step using the trimer ($N = 3$). Namely, we diagonalise the timer using a relatively small number $m_A^{(0)}$ of states in the system block, and a large number of states $m_B^{(0)}$ in the middle block. A reduced density matrix is then formed for the middle unit (by performing a partial trace over the system and environment block Hilbert spaces on an appropriate projection operator) and diagonalised to give the basis used for middle units in the subsequent DMRG iterations.

Fig. 2 shows a DMRG iterative step in the infinite lattice algorithm.

1. First, a system block and its reflection are combined without a middle unit in order to treat systems with an even number of repeat units. In this calculation $m_A^{(1)}$ states are retained in the blocks.

2. Next, a middle unit is inserted in the superblock. However, we perform two further basis optimisations to improve the middle block and system block bases in the context of this system size before obtaining our final energy estimates.

3. In the first step we improve the middle block basis (obtained from the trimer calculation depicted in Fig. 1) by again retaining a relatively small number $m_A^{(2)}$ states in the system and environment blocks and a relatively large number $m_B^{(2)}$ states in the middle block, with $m_B^{(2)} \leq m_B^{(0)}$. A reduced density matrix is again formed for the middle block and diagonalised to give an improved middle block basis for this system size.

4. A similar optimisation is then carried out for the system block, this time keeping a relatively small number of states $m_B^{(3)}$ in the middle unit and a relatively large number of states $m_A^{(3)}$ in the system and environment blocks. A reduced density matrix is formed for the system block by tracing out over the middle unit and environment block spaces.

5. Finally, the energy estimates are obtained for this system size by retaining $m_A < m_A^{(3)}$ states from the reoptimised system block basis and $m_B < m_B^{(2)}$ states from the optimised middle block basis. It is also at this stage that the system block and middle unit are augmented to produce the system block used in the next iteration.

Before discussing our results, we assess the convergence of the DMRG procedure with m_A and m_B. We first consider the noninteracting limit ($U = 0$) where comparisons can be made with exact results. Table I shows the energies obtained for a number of states in various symmetry channels for $N = 11$ phenyl rings using $m_A = 280$ and $m_B = 468$. In this example $m_A^{(0)} = 112$ and $m_B^{(0)} = 606$ and the extra middle unit and system block optimisations ((b) and (c) in Fig. 2) are not used. The accuracy varies with the state studied but even the most inaccurate state is resolved to within 0.02 eV. These results are a number of orders of magnitude more accurate than a previous effort to apply the DMRG to the oligo-phenylene geometry [15].

In the interacting case of interest the convergence of energies is monitored as a function of both m_A and m_B. We first consider biphenyl ($N = 2$) in order to get an idea of the efficiency of the phenyl bases. In Table II we list

the energies of the two lowest $^1A_g^+$ states as functions of $m_A^{(1)}$, the number of system block states retained in step (a) of the procedure depicted in Fig. 2. The indication is that even around 100 states around 3% of the total basis gives a reasonably accurate truncated basis for the phenyl block. We next consider the initial trimer step ($N = 3$) depicted in Fig. 1. In Table III we list results for the $2^1A_g^+$ transition energy as a function of $m_A^{(0)}$ and $m_B^{(0)}$. The energy is converged to within around 0.01 eV. We have found that, once this initial reoptimisation of the middle phenyl block has been done for the trimer system, the parameter that controls the convergence (the parameter to which the energies are most sensitive) is the usual DMRG truncation parameter m_A, the number of states retained in the system and environment blocks. A typical example is given in Table IV where the $2^1A_g^+$ energy state is listed for various m_A and m_B. The value of $m_A^{(0)}$ is set at 140 throughout, the value of $m_B^{(0)}$ is varied with m_B as shown, and the extra middle unit and system block optimisations (steps (b) and (c) from Fig. 2) are not used. The results indicate that the $2^1A_g^+$ energy is resolved to within around 0.02 eV or better.

In production calculations we use all the embellishments depicted in Fig. 2. A typical example of the parameters used is given by: $m_A^{(0)} = 168$, $m_B^{(0)} = 1000$, $m_A^{(1)} = 340$, $m_A^{(2)} = 140$, $m_B^{(2)} = 740$, $m_A^{(3)} = 290$, $m_B^{(3)} = 300$, $m_A = 180$ and $m_B = 520$. We have not carried out a comprehensive study of the effect of the embellishments (b) and (c) but, from running a few sets of parameters for the same target states, and from observing the change in energy obtained from using a reduced, reoptimised basis for either the system block or the middle phenyl unit, the indication is that they allow us to work with effectively larger values of m_A and m_B. That is, using the embellished procedure with the above parameter set is probably equivalent to the simpler scheme (without steps (b) and (c)) with $m_A \approx 290$ and $m_B \approx 740$. We are fairly confident that, in the calculations in this paper, the lowest lying eigenstates in a given symmetry channel are resolved to within around 0.02 eV or better [16].

We now turn to a discussion of our results. We first embark on an investigation of the four characteristic absorption peaks of poly(phenylene) oligomers [17,18] and thin film polymers [17,19,20]. Since the excitations of biphenyl ($N = 2$) are relatively well understood, a knowledge of their evolution with chain length enables us to identify the key excitations in poly-phenyls. As the oligophenyls possess D_{2h} symmetry, the dipole-active states are polarised either along the long axis ($^1B_{1u}^-$) or short axis ($^1B_{2u}^-$). Fig. 3 shows the N-dependence of transition energies of some key states, along with experimental results for biphenyl ($N = 2$) (see [8]), oligomers ($N = 3, \ldots, 6$ [17] and $N = 6$ [18]) and polymer thin films ($N = \infty$) [17,19,20]. We note that the particle-hole dipole-forbidden state ($1^1B_{2u}^+$) lies below the dipole-active $1^1B_{1u}^-$ state in biphenyl. However, the $1^1B_{2u}^+$ state very weakly hybridises, and thus its energy is almost independent of chain length, converging to 4.4 eV. This energy agrees very well with the very weak second absorption peak at 4.4–4.5 eV [19,20] in polymer thin films. Adding weight to this interpretation is the observation of a weak but well defined 4.40 eV absorption peak in a highly textured film of sexiphenyl ($N = 6$), orientated perpendicular to the substrate [18,21], as well as the weak, perpendicularly polarised absorption peak detected in orientated PFO film in the region 4.2–4.8 eV [22]. In contrast, the $1^1B_{1u}^-$ state strongly delocalises. As can be seen from Fig. 3, our DMRG results for the $1^1B_{1u}^-$ in the $N = 3, \ldots, 6$ systems practically coincide with oligomer data [17,18]. For large N the $1^1B_{1u}^-$ energy approaches 3.73 eV in reasonable agreement with the experimental peak observed at 3.63–3.68 eV [17,20], or 3.2 eV [19]. Together these results indicate that the first (strong) and second (weak) absorption peaks in phenyl-based systems are the $1^1B_{1u}^-$ and $1^1B_{2u}^+$ states, respectively.

The third and fourth absorption peaks are polarised normal ($^1B_{2u}^-$) and parallel ($^1B_{1u}^-$) to the long axis, respectively. In thin films they lie at 5.2–5.3 eV [19,20] and 5.7–6.0 eV [19,20] respectively. The $^1B_{1u}^-$ state is a localised intra-phenyl (Frenkel) excitation which lies at 6.16 eV in biphenyl [8]. To track the position of this state as a function of N, we perform calculations targeting a number of $^1B_{1u}^-$ states together with the ground state $1^1A_g^+$ and calculate the dipole moments $\langle 1^1A_g^+|\hat{\mu}|j^1B_{1u}^-\rangle$, where $\hat{\mu} \equiv \sum_i x_i n_i$ (with x_i the x coordinate of the ith atom) is the dipole operator along the long molecular axis. A typical set of dipole moments, for $N = 8$, is given in Table V. In general, it is found that there are two $^1B_{1u}^-$ states that are strongly dipole connected to the ground state. The first is the $1^1B_{1u}^-$, i.e., the first absorption peak. The second is the localised intra-phenyl excitation, i.e., the fourth absorption peak. (In the $N = 8$ case this is the $5^1B_{1u}^-$ state.) The N-dependence of this high-lying, strongly dipole connected $^1B_{1u}^-$ state is plotted in Fig. 3.

A conspicuous failure of the P-P-P model is its prediction for the remaining state, namely the lowest lying $^1B_{2u}^-$ state. The exact solution for biphenyl places this state at 6.66 eV, whereas experimentally it is at ca. 5.85 (and below the $2^1B_{1u}^-$ state). As shown in Fig. 3 its calculated energy is 5.9 eV in the long chain limit, 0.6–0.7 eV higher than the experimental value. Recent work has shown that the predicted energy of this state is improved if dielectric screening is introduced into the Ohno interaction [23].

Fig. 3 also shows the lowest lying triplet ($1^3B_{1u}^+$) and the dipole-forbidden $2^1A_g^+$ state. Electroabsorption studies place the $2^1A_g^+$ state at around 4.6 eV [20,24], around 0.5 eV below the extrapolated P-P-P result of 5.1 eV. (A more recent study [19] places the $2^1A_g^+$ substantially lower). This discrepancy might possibly be explained in

terms of the characteristic red shifts generally observed for certain excited states when going from well isolated chains to polymers in the solid state. Typical estimates for this polarisation or interchain screening shift are ca. 0.3 eV for the $^1B^-_{1u}$ state and ca. 0.6 eV for the $2^1A^+_g$ [25]. As can be seen from Table V the $2^1A^+_g$ state has a large dipole moment with the $1^1B^-_{1u}$ state, and unlike the case for polyenes, it is not pre-dominantly a pair of bound magnons, but a particle-hole excitation. (It is usually labelled the $m^1A^+_g$ state.) This particle-hole excitation is either a 'p'-wave exciton, or the edge of the unbound particle-hole continuum.

To investigate this further, and the nonlinear optical properties of poly(phenylene) in general, we consider dipole moments between various $^1A^+_g$ states and the $1^1B^-_{1u}$ state, as well as between the $2^1A^+_g$ state and various $^1B^-_{1u}$ states. The $N = 8$ values, listed in Table V, are representative of the general situation. We note that, in addition to the $1^1A^+_g$ and $2^1A^+_g$, another, higher lying state, which we denote the $k^1A^+_g$, also has an appreciable dipole moment with the $1^1B^-_{1u}$. (For the $N = 8$ case $k = 5$.) We also observed a pattern in the $\langle 2^1A^+_g|\hat{\mu}|j^1B^-_{1u}\rangle$ values. Namely, the $j = 1$ state has a strong dipole moment with the $m^1A^+_g$, as does the higher lying $^1B^-_{1u}$ absorption peak state (localised intra-phenyl exciton). In addition, there is another state, lying higher still, that has the largest dipole moment with the $m^1A^+_g$. We adopt the usual convention of denoting this state as the $n^1B^-_{1u}$. (In the $N = 8$ case $n = 7$.)

In Fig. 4 we plot a number of $^1A^+_g$ and $^1B^-_{1u}$ state transition energies as functions of $1/N^2$ [26]. We see that there are a number of states in the $^1B^-_{1u}$ sector which seem to converge to the same energy as the $1^1B^-_{1u}$ in the bulk limit. This is the band of 's'-wave charge-transfer excitons. Similarly, the $m^1A^+_g$ (i.e., the $2^1A^+_g$) has a number of momentum branches converging to the same energy, which is the band of 'p'-wave charge-transfer excitons. Above this lies the localised intra-phenyl $^1B^-_{1u}$ state [28]. Higher in energy still are the $k^1A^+_g$ and the $n^1B^-_{1u}$ which appear to converge to the same energy in the $N = \infty$ limit. The strong dipole moments from the $m^1A^+_g$ to the $n^1B^-_{1u}$ and the $1^1B^-_{1u}$ to the $k^1A^+_g$, and the close proximity in energy of the $k^1A^+_g$ and the $n^1B^-_{1u}$ states indicate that these mark the onset of the continuum of unbound particle-hole excitations. Lying below this continuum are the 's'- and 'p'-wave charge-transfer excitons and the Frenkel exciton. This hypothesis could be checked further by calculating the average particle-hole separation for the various states to see if the $n^1B^-_{1u}$ is the first unbound state in the $^1B^-_{1u}$ sector. The convergence of the $k^1A^+_g$ and the $n^1B^-_{1u}$ energies to ca. 6.25 eV as $N \to \infty$ would imply a very large binding energy (ca. 2.5 eV) for the $^1B^-_{1u}$ exciton. However, band states are generally expected to be strongly effected by solid state screening (a red shift of 1.5 eV has been estimated for polyacetylene [25]). Taking such a shift into account would bring the $n^1B^-_{1u}$ and hence the exciton binding energy much closer to the results implied by electroabsorption experiments [19].

In conclusion, we used a π-electron model to investigate the excited states of poly(phenylene), a model light emitting polymer. The transition energies were calculated using a new DMRG method. In order to accomodate the large repeat unit in the DMRG calculation, a truncated local Hilbert space was constructed for the phenyl unit. Using an optimal (or 'natural') basis affords us convergence in the excitation energies to within a small fraction of an eV. For the most part, the calculated transition energies agree well with the experimental results for biphenyl. By monitoring the evolution of the energies with chain length and comparing them to the experimental absorption peaks of oligomers and thin film polymers, we can assign the four characteristic absorption peaks of phenyl-based light emitting polymers. In ascending order they are the $1^1B^-_{1u}$, $1^1B^+_{2u}$, $1^1B^-_{2u}$ and a high lying, localised intra-phenyl (Frenkel exciton) $1^1B^-_{1u}$ state. A failure of the P-P-P model is the incorrect prediction that the $1^1B^-_{2u}$ state lies above the Frenkel exciton [29]. We have also investigated the finite-size scaling of the nonlinear optical states in the longitudinally polarised one- ($^1B^-_{1u}$) and the two- ($^1A^+_g$) photon sectors and found evidence for two $^1B^-_{1u}$ and one $^1A^+_g$ excitonic bands lying below the continuum.

Computations were performed at the New South Wales Center for Parallel Computing, The Australian Center for Advanced Computing and Communications and The Australian Partnership for Advanced Computation. Dr Bursill was supported by The Australian Research Council and The J. G. Russell Foundation.

---

* Email address: ph1rb@phys.unsw.edu.au
** Email address: W.Barford@sheffield.ac.uk

[1] R. H. Friend *et al.*, Nature **397**, 121 (1999).
[2] P. Gomes da Costa and E. M. Conwell, Phys. Rev. B **48**, 1993 (1993); R. Kersting *et al.*, Phys. Rev. Lett. **73**, 1440 (1994); M. Chandross *et al.*, Phys. Rev. B **50**, 14702 (1994); J. M. Leng *et al.*, Phys. Rev. Lett. **72**, 156 (1994); E. M. Conwell *et al.*, *ibid* **73**, 3179 (1994); J. M. Leng *et al.*, *ibid* **73**, 3180 (1995); S. Barth and H. Bassler, *ibid* **79**, 4445 (1997); D. Moses *et al.*, *ibid* **80**, 2685 (1998); S. F. Alvarado *et al.*, *ibid* **81**, 1082 (1998); V. I. Arkhipov *et al.*, *ibid* **82**, 1321 (1999).
[3] M. Chandross *et al*, Phys. Rev. B **55**, 1486 (1997).
[4] M. Chandross and S. Mazumdar, Phys. Rev. B **55**, 1497 (1997).
[5] M. J. Rice and Yu. N. Gartstein, Phys. Rev. Lett. **73**, 2504 (1994); Yu. N. Gartstein, M. J. Rice and E. M. Cornwell, Phys. Rev. B **52**, 1683 (1995); N. Kirova, S. Brazovskii and A. R. Bishop, Synth. Met. **100**, 29 (1999); *ibid* **101**, 271 (1999).

[6] J. D. Weibel and D. Yaron, unpublished.
[7] R. Pariser and R. G. Parr, J. Chem. Phys. 21 (1953) 446; J. A. Pople, Trans. Faraday Soc. 42 (1953) 1375.
[8] R. J. Bursill, C. Castleton, W. Barford, Chem. Phys. Lett. **294**, 305 (1998).
[9] S. Ramasesha, D. S. Galvao and Z. G. Soos, J. Phys. Chem. **97**, 2823 (1993); A. Chakrabarti and S. Ramasesha, Int. J. of Quant. Chem. **60**, 381 (1996); Z. G. Soos, S. Ramasesha, D. S. Galvão and S. Etemad, Phys. Rev. B **47** 1742 (1993).
[10] S. R. White, Phys. Rev. Lett. **69**, 2863 (1992); Phys. Rev. B **48**, 10345 (1993).
[11] D. Yaron, E. E. Moore, Z. Shuai, J. L. Bredas, J. Chem. Phys. **108**, 7451 (1998); G. Fano, F. Ortolani, L. Ziosi, J. Chem. Phys. **108**, 9246 (1998); R. J. Bursill and W. Barford, Phys. Rev. Lett. **82**, 1514 (1999); W. Barford, R. J. Bursill and M. Yu. Lavrentiev, Phys. Rev. B **63**, 195108 (2001); A. Race, W. Barford and R. J. Bursill, Phys. Rev. B **64**, 35208 (2001).
[12] W. Barford, R. J. Bursill and M. Yu. Lavrentiev, cond-mat/0003189.
[13] C. Zhang, E. Jeckelmann and S. R. White, Phys. Rev. Lett. **80**, 2661 (1998).
[14] R. J. Bursill, Phys. Rev. B **60**, 1643 (1999); R. J. Bursill, R. H. McKenzie and C. J. Hamer, Phys. Rev. Lett. **80**, 5607 (1998); *ibid*, **83**, 408 (1999).
[15] Y. Anusooya, S. K. Pati and S. Ramasesha, J. Chem. Phys. **106**, 10230 (1997).
[16] Although extensive convergence tests have not been carried out for the even N cases, in the noninteracting limit ($U = 0$) agreement with exact results is as good as that obtained for the case of odd N (see Table I). Further, in the interacting case, energies are found to be smooth functions of N, so we are reasonably confident that our results for even N are comparable in accuracy to those for odd N.
[17] A. Niko *et al.*, Synth. Met. **101**, 662 (1999).
[18] E. Zojer *et al.*, Phys. Rev. B **61**, 16538 (2000).
[19] A. J. Cadby *et al.*, Phys. Rev. B **62**, 15604 (2000); H. Mellor, Ph. D. thesis, University of Sheffield 2000.
[20] P. A. Lane *et al.*, Synth. Met. **84**, 641 (1997).
[21] Although the $1^1B^+_{2u}$ state is particle-hole dipole forbidden in the P-P-P model, it is (weakly) observable in biphenyl (and presumably larger systems) due the fact that particle-hole symmetry is actually broken in real systems. Another possible interpretation of the second absorption peak is that it is due to the $2^1B^-_{1u}$ (see [3]). That is, although the $2^1B^-_{1u}$ and $1^1B^-_{1u}$ coincide in the $N = \infty$ limit (see Fig. 4), for systems of around $N = 8$ phenyl rings, the $2^1B^-_{1u}$ has an appreciable dipole moment with the $1^1A^+_g$ (see Table V) and has an energy of around 4.4 eV. Although it is argued that this scenario is ruled out by polydispersity [6], this alternative interpretation is possible if we assume that the conjugation length distribution is sharply peaked around $N = 8$ rings in thin films (i.e. unlike the $1^1B^+_{2u}$, the $2^1B^-_{1u}$ has strong N-dependence). Interestingly, beyond the first maximum centered at 3.95 eV, in addition to the short-axis polarised peak at 4.4 eV, the long-axis polarised absorption in [18] shows a peak at 4.91 eV that agrees well with the P-P-P $2^1B^-_{1u}$ result of 4.88 eV for $N = 6$ (see Fig. 4).
[22] E. K. Miller *et al.*, Phys. Rev. B **60**, 8028 (1999).
[23] C. Castleton and W. Barford, unpublished.
[24] It is usually assumed that the $2^1A^+_g$ state is a spin-density wave, (as is the case for the dimerised Hubbard model in the strongly correlated regime) and hence does not contribute to the nonlinear optical spectra. In this case, however, the $2^1A^+_g$ has a large dipole moment with the $1^1B^-_{1u}$, and should thus be the $m^1A^+_g$ state visible in electroabsortion.
[25] E. E. Moore and D. Yaron, J. Chem. Phys. **109**, 6147 (1998).
[26] We note that, whilst for small N, energies are fairly linear in $1/N$ (see, e.g., the theoretical and experimental $1^1B^-_{1u}$ results in Fig. 3), for large N, energies are linear in $1/N^2$ [27]. This fact can be used to easily obtain extrapolations to the bulk limit ($N = \infty$): straightforward linear extrapolation in $1/N^2$ gives estimates of the bulk energies within confidence limits dictated by the DMRG truncation error (around 0.02 eV).
[27] R. J. Bursill, E. Jeckelmann and W. Barford, unpublished.
[28] We have seen some evidence of a band of states at this energy but it will be necessary to target a number of states in this energy range explicitly in order to clearly see higher momentum branches of the localised intra-phenyl $^1B^-_{1u}$ exciton.
[29] Although the positions of these states can be inverted by reducing the electron correlation [3] (the parameters in [3] were determined within CI theory), or by the use of more phenomenological, semi-analytic approaches and a number of fitting parameters [5], our philosophy here has been to develop a numerical scheme that can first determine the predictions of P-P-P theory (without adjustable parameters or uncontrolled approximations), before embarking on the task of attempting to improve it.

TABLE I. Comparison of DMRG and exact results for the $N = 11$ phenyl oligomer in the noninteracting ($U = 0$) limit. In the DMRG calculations $m_A = 280$ and $m_B = 468$.

	$E(1^1A^+_g)$	$E(1^1B^-_{1u})$	$E(2^1A^+_g)$	$E(1^1B^-_{2u})$
DMRG	−231.0210234	−228.4828	−228.331	−227.195
EXACT	−231.0210256	−228.4832	−228.328	−227.213

TABLE II. Convergence of the lowest two states in the $^1A^+_g$ sector with $m^{(1)}_A$ for biphenyl ($N = 2$).

$m^{(1)}_A$	$E(1^1A^+_g)$	$E(2^1A^+_g)$
34	−63.0095953	−56.7041530
92	−63.0125556	−56.7137143
140	−63.0126802	−56.7140886
188	−63.0126995	−56.7141368
260	−63.0127066	−56.7141589
322	−63.0127078	−56.7141631
exact	−63.0127086	−56.7141653

TABLE III. Convergence of the two-photon ($2^1A_g^+$) state transition energy with the DMRG parameters $m_A^{(0)}$ and $m_B^{(0)}$ for the trimer ($N = 3$).

$m_B^{(0)}$	$m_A^{(0)} = 34$	$m_A^{(0)} = 92$	$m_A^{(0)} = 140$
420	5.7626	5.7498	5.7486
574	5.7578	5.7449	5.7437
692	5.7562	5.7433	5.7421
952	5.7544	5.7415	5.7405

TABLE IV. Convergence of the two-photon ($2^1A_g^+$) state transition energy with the DMRG parameters m_A and m_B for the $N = 11$ system.

m_B	$m_B^{(0)}$	$m_A = 34$	$m_A = 85$	$m_A = 130$	$m_A = 165$
34	140	5.38712	5.35049	5.36911	5.36862
92	204	5.23364	5.17443	5.19057	5.18949
140	322	5.21740	—	5.16678	5.16533
202	420	5.20744	—	5.15356	5.15170
268	574	5.20605	5.17076	5.15089	5.14903
346	692	5.20490	5.16566	5.14948	5.14757
418	848	5.20441	5.16545	5.14901	5.14715
468	952	—	5.16525	—	5.14696

TABLE V. Dipole moments connecting various $^1A_g^+$ and $^1B_{1u}^-$ states for the $N = 8$ system.

j	$\langle 1^1A_g^+ \vert\hat{\mu}\vert j^1B_{1u}^- \rangle$	$\langle j^1A_g^+ \vert\hat{\mu}\vert 1^1B_{1u}^- \rangle$	$\langle 2^1A_g^+ \vert\hat{\mu}\vert j^1B_{1u}^- \rangle$
1	2.85	2.85	2.64
2	0.68	2.64	0.48
3	0.19	0.31	0.06
4	0.11	0.14	0.02
5	2.52	1.17	1.57
6	1.03	—	1.31
7	0.62	—	5.06
8	0.48	—	0.04

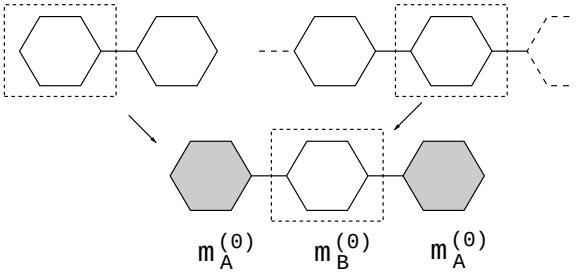

FIG. 1. The initial step in developing the optimised phenyl block bases used in subsequent DMRG iterations. Dashed lines indicate the formation of reduced density matrices.

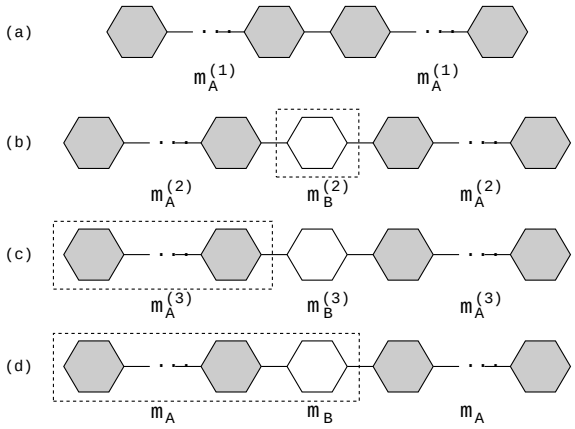

FIG. 2. The steps involved in a DMRG iteration: (a) Two system blocks are combined in order to treat systems with even N; (b) The middle phenyl unit basis is reoptimised in the context of this system size; (c) The system block is reoptimised for this superblock; (d) The final energy estimates are made, and the system block is augmented to produce the system block used in the next DMRG iteration. Dashed lines indicate the formation of reduced density matrices.

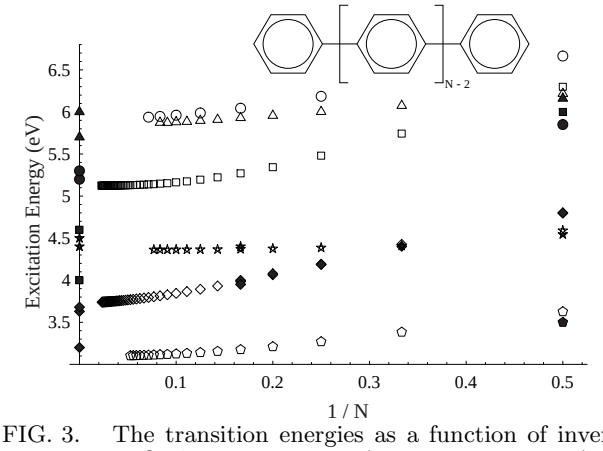

FIG. 3. The transition energies as a function of inverse chain length: $1^3B_{1u}^+$ (pentagons), $1^1B_{1u}^-$ (diamonds), $1^1B_{2u}^+$ (stars), $2^1A_g^+$ (squares), $1^1B_{2u}^-$ (circles) and the localised intra-phenyl $^1B_{1u}^-$ (Frenkel) state (triangles). The filled symbols are the experimental values for biphenyl (see ref. [8]), oligomers ($N = 3, \ldots, 6$ [17] and $N = 6$ [18]) and thin film polymers ($N = \infty$) [17,19,20]. The inset shows the oligo-phenylene geometry.

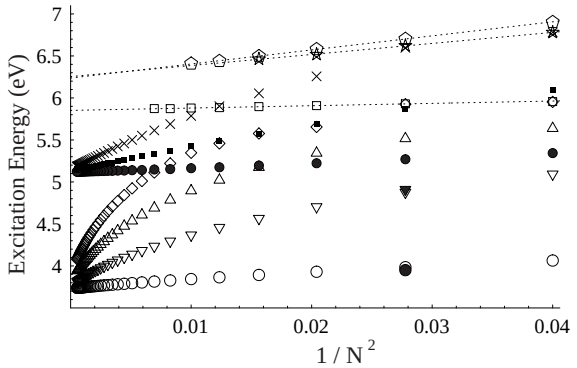

FIG. 4. The transition energies of a number of ${}^1A_g^+$ and ${}^1B_{1u}^-$ states as a function of $1/N^2$, where N is the number of repeat units: $1{}^1B_{1u}^-$ (large, open circles), $2{}^1B_{1u}^-$ (open, down triangles), $3{}^1B_{1u}^-$ (up triangles), $4{}^1B_{1u}^-$ (diamonds), the high lying localised intra-phenyl ${}^1B_{1u}^-$ excitation (open squares), $n{}^1B_{1u}^-$ (pentagons), $m = 2{}^1A_g^+$ (small, solid circles), $3{}^1A_g^+$ (small, solid squares), $4{}^1A_g^+$ ($\times$) and $k{}^1A_g^+$ (stars). The large, solid circle and solid down triangle show the position of the first and second long-axis polarised absoprtion peaks respectively for sexiphenyl ($N = 6$) [18,21]. The dotted lines are to guide the eye.